JANOLI International Journal of
Physics
(A Peer Review Journal)

journal homepage:https://janolijournals.com/index.php/jijp/index

Volume 2, Issue 1, Jan- 2026 ISSN: 3107-4561

Constraining the Extragalactic Background Light (EBL) using the 50-MGC Galaxy Catalog

Brizuela, Manuel
Falcón, Nelson

Laboratory of Atmospheric Physics and Outer Space, FACYT Physics Dept.
Universidad de Carabobo. Valencia, Edo. Carabobo, Venezuela.
brizuela.manuelj@gmail.com nelsonfalconv@gmail.com

ARTICLE INFO

Article History:
Received March 10, 2026
Revised March 10, 2026
Accepted March 15, 2026
Available online March 25, 2026

Keywords:
Extragalactic background light, Olbers' Paradox, galaxies: stellar content, nearby galaxies.

Correspondence:
E-mail:
brizuela.manuelj@gmail.com
, nelsonfalconv@gmail.com

ABSTRACT

This study quantitatively restricts Olbers' Paradox by evaluating the intensity of the extragalactic background light (EBL) in the optical B-band. Utilizing the 50-MGC galaxy catalog, we establish the numerical densities and intrinsic luminosities of nearby galaxies. To construct a physical model, the local galactic demography was decoupled into star-forming and quiescent populations, evaluating their distinct stellar content. By applying stellar population synthesis and empirical mass assembly metrics, we modeled the continuous evolution of these populations across cosmic time. The comoving numerical density and mean luminosity functions were integrated over redshift to compute the total radiative flux across varying Hubble parameter values (H0)—representing the Planck, Riess, and GM-UYF frameworks—while maintaining constant matter-energy densities. The results demonstrate that while assuming a constant numerical density and luminosity yields fluxes within observational limits, this approach is severely biased. Conversely, extrapolating local redshift-dependent regressions severely underestimates the optical background. We conclude that incorporating decoupled galactic evolution, alongside a galactic extinction filter ($|b|>45$), is necessary to reconcile theoretical EBL fluxes with empirical limits, successfully resolving the divergent integral of Olbers' Paradox.

1.Introduction

The Extragalactic Background Light (EBL) is the cumulative radiative flux originating from all astrophysical sources throughout cosmic history. In observational cosmology, calculating the precise intensity of the optical EBL is a fundamental requirement to achieve a quantitative resolution to Olbers' Paradox.

Historically, M. Olbers [1] noted that in an infinite, static, and uniform universe, the night sky should be fully illuminated, reasoning geometrically that the number of stars in concentric spherical shells increases at the same rate their individual brightness decreases. The modern mathematical formulation of this

paradox assumes a constant number density of light sources, n_0, and a constant mean luminosity, $\langle L \rangle$. The radiative flux f received from a single star at a distance r from Earth is given by the inverse-square law:

$$f(r) = \frac{\langle L \rangle}{4\pi r^2} \tag{1}$$

The number of stars dN located within a spherical shell of thickness dr at a distance r from Earth is $dN = n_0(4\pi r^2)dr$. Consequently, the total radiative flux of the sky $\mathcal{F}$ is the integral of the individual flux multiplied by the number of sources:

$$\mathcal{F} = \int_0^\infty f(r)dN = \int_0^\infty \frac{\langle L \rangle}{4\pi r^2}(n_0 4\pi r^2)dr = \int_0^\infty n_0 \langle L \rangle dr \to \infty \tag{2}$$

This integral diverges, leading to the incorrect prediction of an infinitely bright sky.

Modern cosmology resolves this paradox qualitatively through the expansion of the universe and its finite age, which prevent the integral from extending to infinity. At the stellar level, Lord Kelvin [2] argued that stars have a finite lifespan, meaning their emitted light is limited. However, when applied to galaxies, this argument falls short: galaxies do not "die" quickly; they undergo continuous cycles of star formation over billions of years. Therefore, accurately computing the EBL requires modeling the demographic evolution and star-formation history of galaxies rather than treating them as simple, static light sources.

Recent observational projects have established tight constraints on the actual intensity of the EBL. Lauer et al. [3] measured the optical background using the New Horizons spacecraft beyond Pluto, thereby avoiding the intense Zodiacal Light that blinds telescopes near Earth. Similarly, Mattila et al. [4] isolated the EBL using the shadows of dark interstellar clouds. Other programs, such as SKYSURF [5], have constrained the Integrated Galactic Light (IGL) using archival images from the Hubble Space Telescope.

While these observational efforts provide empirical limits, verifying these results requires robust theoretical and computational models. The objective of this paper is to quantitatively restrict Olbers' Paradox by computing the optical EBL (specifically in the B-band). To achieve this, we utilize the 50 Mpc Galaxy Catalog (50-MGC) [6] to establish the initial numerical densities and average luminosities in the local universe. We then classify the catalog into star-forming (SF) and quiescent (Q) populations to apply appropriate evolutionary functions across cosmic time and compute the total integrated flux.

This paper is organized as follows: Section 2 presents the theoretical foundations; Section 3 details the methodology, including the processing of the 50-MGC catalog and the SF/Q decoupling; Section 4 presents the analytical results and evaluates the EBL under standard cosmological parameters; and Section 5 discusses the conclusions.

2.Theoretical Foundations

The radiative flux f received on Earth from a single galaxy with an intrinsic, redshift(z)-dependent mean luminosity $\langle L(z) \rangle$ is inversely proportional to the square of its luminosity distance d_L:

$$f(z) = \frac{\langle L(z) \rangle}{4\pi d_L^2} \tag{3}$$

The luminosity distance d_L is related to the comoving radial distance r and the redshift z by $d_L = a_0 r(1 + z)$, where a_0 is the present-day cosmic scale factor. The differential number of galaxies dN located in a spherical shell of proper volume dV between redshift z and $z + dz$ is determined by the proper number density $n_{prop}(z)$:

$$dN = n_{prop}(z)dV \tag{4}$$

The differential proper volume element at the epoch of emission is defined by the scale factor a as $dV = 4\pi(ar)^2(adr) = 4\pi a^3 r^2 dr$. Due to the expansion of the universe, and assuming galaxies behave as a pressureless dust fluid, their physical number density dilutes inversely with the cosmic volume. Thus, the proper number density relates to the comoving number density $n(z)$ by the volume ratio $(a_0/a)^3$:

$$n_{prop}(z) = n(z)\left(\frac{a_0}{a}\right)^3 \tag{5}$$

Substituting these expressions, the emission scale factor a mathematically cancels out. The differential number of sources is then expressed purely in terms of the comoving density and the present-day scale factor a_0:

$$dN = \left[n(z)\left(\frac{a_0}{a}\right)^3\right]\left(4\pi a^3 r^2 dr\right) = 4\pi n(z) a_0^3 r^2 dr \tag{6}$$

To determine the differential coordinate dr, a change of variable is performed from dr to cosmic time dt, and subsequently from dt to redshift dz. For a photon traveling radially toward the observer, the comoving distance element is $dr = \frac{c}{a}dt$. By applying the cosmic scale relation $(1 + z) = a_0/a$, this can be rewritten as $dr = \frac{c(1+z)}{a_0}dt$, where c is the speed of light in vacuum. The relation between cosmic time and redshift is derived from the Hubble parameter $H(z) = \dot{a}/a$, yielding $dt = -\frac{dz}{H(z)(1+z)}$. Combining these expressions, the differential comoving radial coordinate becomes:

$$dr = -\frac{c}{a_0 H(z)}dz \tag{7}$$

The differential radiative flux $d\mathcal{F}_{sky}$ from this shell is the product of the individual flux and the number of sources ($d\mathcal{F}_{sky} = f dN$). Substituting the previous expressions, normalizing by unit solid angle (4π steradians), and simplifying the geometric terms, the differential intensity of the EBL $d\mathcal{F}$ is obtained:

$$d\mathcal{F} = -\frac{c}{4\pi H(z)}\frac{n(z)\langle L(z)\rangle}{(1+z)^2}dz \tag{8}$$

To compute the total intensity, the differential flux is integrated over cosmic time, from the distant past ($z = \infty$) to the present epoch ($z = 0$). The negative sign in the differential element inverts the integration limits. The expansion history of the universe is governed by the redshift-dependent Hubble parameter $H(z) = H_0 E(z)$, where H_0 is the local Hubble constant and $E(z)$ is the dimensionless Hubble parameter. For a spatially flat cosmological model, $E(z)$ is defined by the Friedmann equation as:

$$E(z) = \sqrt{\Omega_m(1 + z)^3 + \Omega_\Lambda} \tag{9}$$

where Ω_m and Ω_Λ correspond to the present-day matter and dark energy density parameters, respectively. Substituting $H(z)$ into the differential flux, the integrated expression for the EBL intensity $\mathcal{F}$ (in W m^{-2} sr^{-1}) is:

$$\mathcal{F} = \frac{c}{4\pi H_0}\int_0^{\infty} \frac{n(z)\langle L(z)\rangle}{(1+z)^2 E(z)} dz \tag{10}$$

Evaluating (10) requires explicit functions for the comoving number density $n(z)$ and the mean luminosity $\langle L(z)\rangle$. Following Peng et al. [7] the galactic population decouples into two distinct evolutionary tracks: star-forming (SF) and quiescent (Q) galaxies, bifurcating the integral into $n_{SF}(z)\langle L_{SF}(z)\rangle$ and $n_Q(z)\langle L_Q(z)\rangle$.

The Stellar Mass Function (SMF), $\Phi(M, z)$, defines the number density of galaxies per unit comoving volume per logarithmic mass interval. The comoving number density $n(z)$ is obtained by integrating the SMF over the relevant range of stellar masses M, where M_{min} and M_{max} denote the lower and upper mass limits of the galaxy population:

$$n(z) = \int_{M_{min}}^{M_{max}} \Phi(M, z) dM \tag{11}$$

By adopting the empirical double-Schechter SMF parameters [8], this integration yields a continuous numerical density function $n(z)$ for both SF and Q populations.
For star-forming galaxies, the optical emission is dominated by massive, short-lived stars. Consequently, the mean luminosity $\langle L_{SF}(z)\rangle$ is directly proportional to the Cosmic Star Formation Rate (CSFR) mass density, $\Psi(z)$ [9]:

$$\langle L_{SF}(z)\rangle \propto \Psi(z) \tag{12}$$

Conversely, quiescent galaxies lack active star formation and are well-represented by Simple Stellar Populations (SSPs) undergoing passive evolution. Their optical luminosity is governed by the progressive aging of intermediate-mass stars. Analytically, the luminosity of an SSP decays as a power law of time, $\langle L\rangle \propto t^{-\gamma}$ [10]. For the B-band, Stellar Population Synthesis models by Bruzual and Charlot [11] restrict this exponent to the range $0.86 \leq \gamma \leq 1.0$, depending on the stellar metallicity [12]. Since the precise metallicity distribution of the local quiescent population is unresolved in integrated surveys, we adopt the arithmetic mean of this theoretical range ($\gamma = 0.93$). Therefore, the mean luminosity evolution of quiescent galaxies is modeled as:

$$\langle L_Q(z)\rangle \propto t(z)^{-0.93} \tag{13}$$

3.Methodology

The 50 Mpc Galaxy Catalog (50-MGC), compiled by Ohlson et al. [6], is a recent survey that offers specific technical advantages for modeling galaxy populations. It is a volume-limited catalog (meaning it provides a statistically complete census of galaxies within a defined spatial boundary). Furthermore, the 50-MGC utilizes redshift-independent distance measurements, a feature that mitigates kinematic biases introduced by local peculiar velocities. The dataset provides the intrinsic B-band luminosities, stellar masses, and morphological types, serving as the basis for the analysis of galaxy distributions. The specific variables extracted from the catalog are listed in Table 1.

Table 1 Key parameters extracted from the 50-MGC dataset for EBL evaluation.

Variable	Description
bestdist	Optimal redshift-independent distance estimate (Mpc).
v_cmb	Radial velocity with respect to the CMB radiation (km s $^{-1}$).
best_type	Combined morphological and color-based classification.
t_type	Numerical Hubble T-Type morphology index.
BMag	Absolute B-band magnitude, corrected for galactic extinction.
B_lum	Intrinsic B-band luminosity ($L_{\odot}$).
logmass	Compiled logarithmic stellar mass estimate ($M_{\odot}$).

The EBL intensity calculation depends on the Hubble parameter (H_0) and the matter-energy density components (Ω_m, Ω_Λ). To isolate the effect of the cosmic expansion rate on the integrated flux, the calculation is performed maintaining the density components constant across all models, adopting the measurements from the Pantheon sample by Scolnic et al. [13] ($\Omega_m = 0.298$, $\Omega_\Lambda = 0.702$). We then evaluate four distinct scenarios for the Hubble parameter. The first scenario adopts the early-universe results from the Planck Collaboration [14], with $H_0 = 67.40$ km s^{-1} Mpc^{-1}. The second utilizes the late-universe local measurements from Riess et al. [15], with $H_0 = 74.03$ km s^{-1} Mpc^{-1}. Finally, we evaluate the alternative modified gravity framework (GM-U_{YF}) developed by Falcón [16], [17], adopting the empirically fitted local slope $H_{0,local} = 70.18$ km s^{-1} Mpc^{-1} [18], alongside its theoretical upper limit $H_{0,upper} = 86.31$ km s^{-1} Mpc^{-1} [16], [17], [18].

Broadly speaking, the local galaxy population exhibits a strong bimodality that correlates morphological structure with star formation history. Elliptical and lenticular galaxies are typically gas-poor, dominated by older stellar populations (Population II), and exhibit redder spectra; these constitute the quiescent (Q) population. In contrast, spiral and irregular galaxies are gas-rich, host active star-forming regions with massive young stars (Population I), and exhibit bluer spectra, forming the star-forming (SF) population. To model the continuous demographic evolution of the universe, we align our analysis with the paradigm established by Peng et al. [7], which evaluates galactic evolution through these two primary tracks (SF and Q) rather than strict morphological types.

To empirically separate these populations within the 50-MGC, we utilize the photometric color-mass diagram. The g (green) and i (near-infrared) bands capture the optical spectral slope, serving as a robust proxy for the age and star formation rate of a galaxy. Rather than establishing new parameters, we directly apply the empirical cuts defined by Ohlson et al. [6], adopting their primary separation line, $(g - i)_{sep}$, and lower reclassification boundary, $(g - i)_{rec}$, in the color-mass plane:

$$(g - i)_{sep} = 0.133 log(M_*/M_{\odot}) - 0.294 \; (g - i)_{rec} = 0.124 log(M_*/M_{\odot}) - 0.344 \tag{14}$$

In these equations, M_* represents the absolute stellar mass of the individual galaxy, and $M_{\odot}$ is the standard solar mass used for normalization. These linear limits account for the well-documented

mass-metallicity relation, where more massive galaxies are intrinsically redder even if they are still forming stars; hence, both equations possess a positive slope. The $(g-i)_{sep}$ threshold acts as the upper boundary for the star-forming "blue cloud", while $(g-i)_{rec}$ defines the lower envelope of the "red sequence". The photometric space bounded between these two equations characterizes the "green valley", a critical transition phase where galaxies undergo active quenching, migrating from the star-forming main sequence to the quiescent state.

Following the principles of Peng et al. [7], galaxy quenching is treated as a transitional process rather than an instantaneous event. Consequently, each galaxy is assigned a fractional weight between 0 and 1 instead of using rigid binary cuts. The probability of a galaxy belonging to the quiescent sequence (w_Q) is determined by interpolating its color across the transition zone defined by the Ohlson boundaries. The complementary weight for the star-forming population is defined as $w_{SF} = 1 - w_Q$. The resulting bimodal classification applied to the 50-MGC sample is illustrated in Fig. 1.

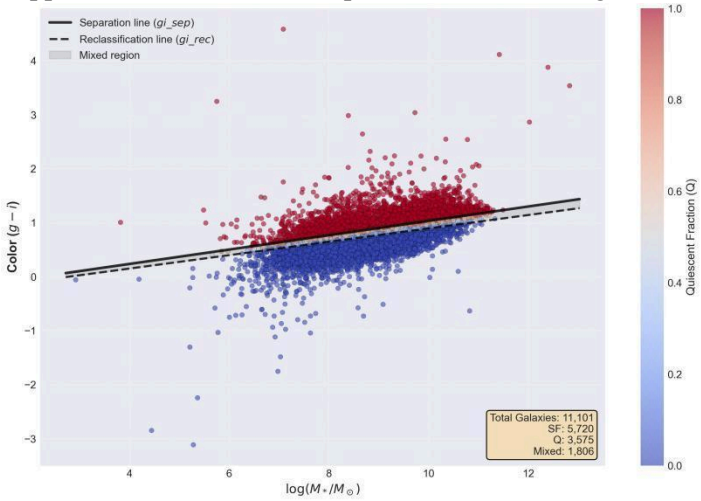

Figure 1 Bimodal color-mass classification of the 50-MGC sample. The solid and dashed lines represent the $(g-i)_{sep}$ and $(g-i)_{rec}$ boundaries, capturing the transition zone between star-forming and quiescent populations. Own elaboration based on [6].

With the populations separated by these weights, the evolutionary functions can be modeled. In this context, the 50-MGC sample can be utilized as an empirical reference at $z \to 0$ ($z \approx 0.012$ at 50 Mpc, assuming the recession velocity v satisfies $v \ll c$) to normalize the theoretical density functions of the deep universe. The comoving numerical densities at $z = 0$ ($n_{0,SF}$ and $n_{0,Q}$) are computed by dividing the weighted galaxy counts by the local spherical volume. Since the double-Schechter models [8] only extend down to $z \approx 0.35$, we perform a linear extrapolation of their integrated density functions to $z = 0$. The resulting models are then multiplied by dimensionless proportionality constants $K_{n,i}$ to strictly match the empirical densities obtained from the 50-MGC. Here, $n_{Ilbert,i}(0)$ represents the theoretical density of population i evaluated at present time ($z = 0$):

$$K_{n,i} = \frac{n_{0,i}}{n_{Ilbert,i}(0)}, \quad for\ i \in \{SF, Q\} \tag{15}$$

A similar normalization is applied to the luminosity functions. The local intrinsic luminosities $\langle L_{0,SF} \rangle$ and $\langle L_{0,Q} \rangle$ are extracted via the weighted arithmetic mean of the B-band luminosities. For quiescent galaxies,

we assume that the average epoch of their transition coincides with the cosmic era of maximum mass assembly. Consequently, the maximum value of the fading quiescent luminosity curve coincides with the global maximum of the star-forming curve. This intersection defines the onset of quiescence, ensuring the progressive decay follows the theoretical power law to match the empirical mean luminosity measured locally ($d \leq 50$ Mpc) in the 50-MGC. In the following expressions, $\Psi(0)$ represents the present-day cosmic star formation rate, and $t(0)$ is the current age of the universe:

$$\langle L_{SF}(z)\rangle = \langle L_{0,SF}\rangle \frac{\Psi(z)}{\Psi(0)} \tag{16}$$

$$\langle L_{Q}(z)\rangle = \langle L_{0,Q}\rangle \left(\frac{t(z)}{t(0)}\right)^{-0.93} \tag{17}$$

4.Results

To evaluate the computational results of the EBL integration, we utilize the empirical boundaries [4]. Through the analysis of the shadows cast by dark interstellar clouds, their study restricts the actual optical background in the B-band, reporting a central value of $\mathcal{F} = 11.6 \pm 4.4\, nW\, m^{-2} sr^{-1}$. From this uncertainty, we adopt the lower limit ($\mathcal{F}_{min} = 7.2\, nW\, m^{-2} sr^{-1}$) and upper limit ($\mathcal{F}_{max} = 16\, nW\, m^{-2} sr^{-1}$) as the fundamental physical criteria for assessing the validity of our evolutionary models.

To model the behavior of the comoving numerical density $n(z)$ in the local universe ($d < 50$ Mpc), the spatial volume up to 50 Mpc was divided into 50 equally spaced concentric spherical shells. The empirical density was calculated for each shell and fitted to the following regression function:

$$n(z) = ae^{-bz-ce^{-dz}} \tag{18}$$

Here, a represents the foundational density scale with units of Mpc^{-3}, while b, c, and d are dimensionless empirical regression coefficients optimized to fit the local data. The regression yielded the parameters: $a \cong 0.331$ Mpc^{-3}, $b \cong 388.8$, $c \cong -19.1$, and $d \cong 16163.5$ with a strong quadratic correlation coefficient. The function (18) successfully captures the continuous density distribution across the shells (Fig. 2).

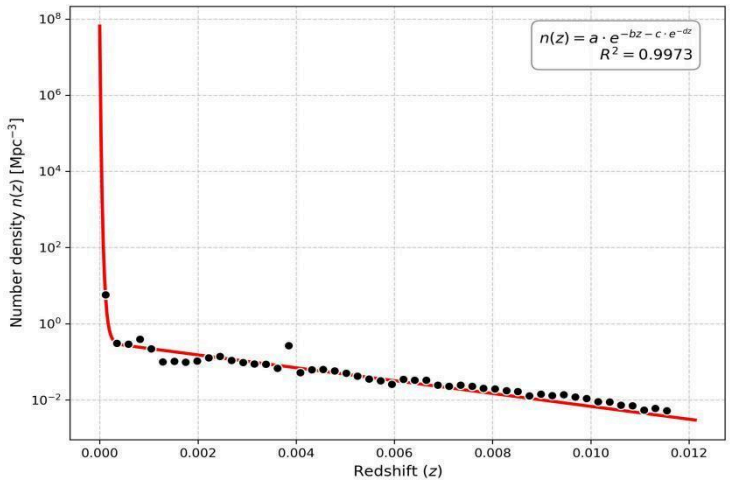

Figure 2 Evolution of the numerical density of galaxies $n_{prop}(z)$ fitted across 50 local shells.

Conversely, the evaluation of the average intrinsic luminosity $\langle L(z) \rangle$ was performed by dividing the volume into 10 shells. This spatial reduction is necessary because, at higher resolutions (e.g., 50 shells), the average luminosity exhibits highly erratic behavior. This instability is dominated by local cosmic variance and selection biases at varying depths, making it difficult to achieve a stable theoretical extrapolation towards the deep universe ($d \gg 50$ Mpc). With 10 shells, the data was smoothed and fitted to the following function:

$$\langle L(z) \rangle = \left[A_1 \left(\frac{z}{z_c} \right)^{a_1} + A_2 \left(\frac{z}{z_c} \right)^{a_2} \right] e^{-z/z_c} \tag{19}$$

In this functional form, A_1 and A_2 act as luminosity amplitude scaling factors with units of solar luminosities ($L_\odot$), a_1 and a_2 are dimensionless exponents governing the power-law slopes for different redshift regimes, and z_c acts as a dimensionless exponential cutoff redshift. The regression yielded $A_1 \cong 8.89 \times 10^9 \, L_\odot$, $a_1 \cong -0.179$, $A_2 \cong 7.43 \times 10^7 \, L_\odot$, $a_2 \cong 5.942$, and $z_c \cong 0.0015$. The resulting curve is presented in Fig. 3.

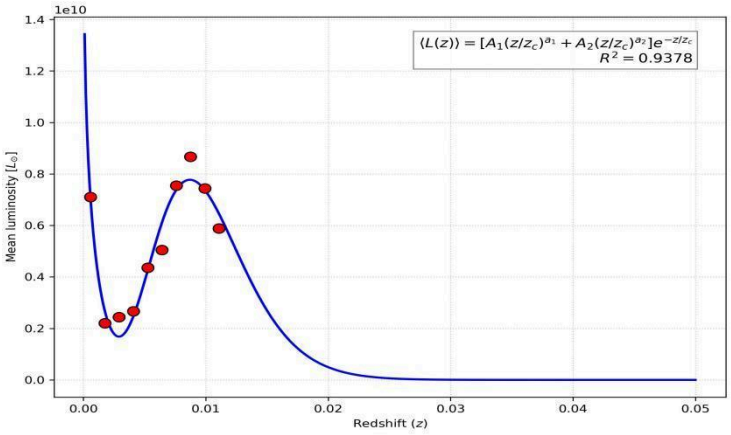

Figure 3 Average luminosity evolution $\langle L(z)\rangle$ fitted across 10 local shells.

By permuting the assumptions of constant local values ($n_0, \langle L_0\rangle$) and evolutionary functions ($n(z), \langle L(z)\rangle$), four primary scenarios were established. The resulting EBL intensities ($\mathcal{F}$) evaluated across the standard ΛCDM parameters (Planck and Riess) and the alternative GM-U_{YF} framework are compiled in Table 2.

Table 2 Integrated EBL intensity $\mathcal{F}$ in different approaches.

Model	H_0 $kms^{-1}Mpc^{-}$	$\mathcal{F}(n_0, L_0)$ $nWm^{-2}sr^{-1}$	$\mathcal{F}(n(z), L_0$ $nWm^{-2}sr^{-}$	$\mathcal{F}(n_0, \langle L(z)$ $nWm^{-2}sr^{-}$	$\mathcal{F}(n(z), \langle L$ $nWm^{-2}sr^{-}$
Planck [14]	67.40	8.588	0.6515	0.2548	0.2759
Riess [15]	74.03	7.819	0.5932	0.2320	0.2512
GM-U_{YF} [18],	70.18	8.248	0.6257	0.2448	0.2650
Upper GM-U_{YF}[16], [17]	86.31	6.706	0.5088	0.1990	0.2155
Lower Limit [4]	-	7.2			
Upper Limit [4]	-	16			

Assuming a constant numerical density and luminosity for the entire universe (Table 2, column 3), the integrated EBL flux falls within the observational limits for the Planck, Riess, and local GM-U_{YF} models. Notably, the Upper GM-U_{YF} limit fails to reach the minimum threshold even under this static assumption. Furthermore, the phenomena of the nearby Universe seem to indicate that this constant assumption is not very realistic. Since the galaxies surveyed, up to 50 Mpc, show a high standard deviation in luminosity values and their three-dimensional distribution is not homogeneous, that is, they do not satisfy the constant n_0.

Then, integrating the EBL using evolutionary global fits ($n(z), \langle L(z)\rangle$) underestimates the optical background by an order of magnitude below the Mattila lower bound across all four evaluated scenarios. This severe underestimation dictates the necessity of implementing the decoupled bimodal model to perform a physically motivated extrapolation towards the deep universe.

The physical extrapolation of the independent comoving densities and mean luminosities are verified in Fig. 4. For the comoving numerical density (left panel), we utilized the integrated double-Schechter

parameters from Ilbert et al. [8]. Since these observational constraints reliably trace mass assembly up to $z \approx 2.75$, an exponential decay function was applied to extrapolate the density of early galaxies beyond this limit. The vertical dashed line explicitly marks this extrapolation boundary, separating the domain of Ilbert's data from the theoretical exponential tail in the early universe.

Regarding the mean luminosity (right panel), the evolution of star-forming (SF) galaxies is modeled to be directly proportional to the Cosmic Star Formation Rate (CSFR) mass density $\Psi(z)$, as defined in Eq.12. Conversely, the quiescent (Q) population luminosity is governed by the passive fading of intermediate-mass stars. As established in Equation 13, this passive decay is modeled following the stellar population synthesis models of Bruzual and Charlot [11]. The vertical line in this panel denotes the transition epoch, corresponding to the global maximum of the star-forming curve. This marks the average quenching point where local quiescent galaxies ceased active star formation and commenced their passive fading phase.

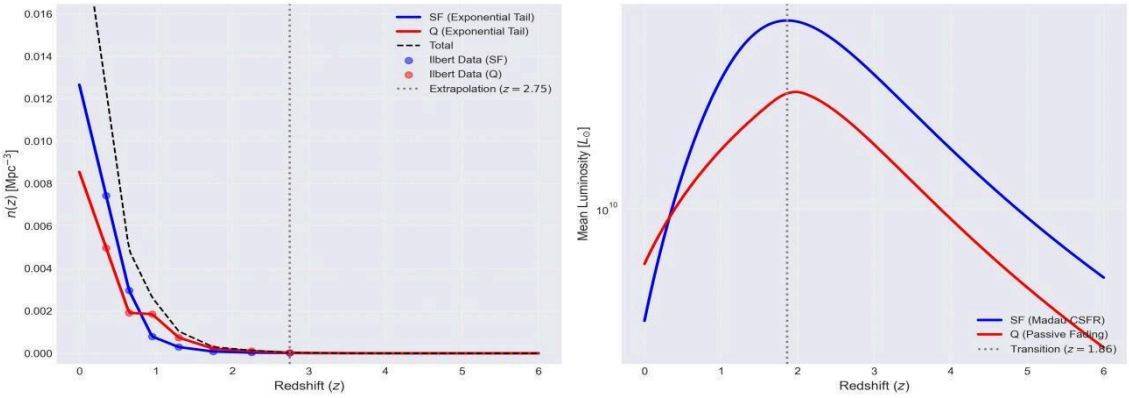

Figure 4 Decoupled evolutionary comoving density (left) and Mean luminosity (right) functions for star-forming and quiescent galaxies.

On the other hand, dust in the Milky Way's disk causes optical extinction in EBL measurements, resulting in a statistical bias that must be considered in the galactic sorting method used. Furthermore, to evaluate the impact of galactic extinction on the observed local counts, the integration was subjected to three distinct spatial filters restricting the galactic latitude ($|b|$). The final computed fluxes utilizing the complete decoupled model are presented in Table 3, when we limit the galactic count to the region near the galactic north, with conic angles: 30° and 45° respects to galactic plane.

Table 3 EBL intensity $\mathcal{F}$ using the bimodal model under galactic latitude filters.

Model	H_0 $kms^{-1}Mpc^{-1}$	Unfiltered $\lvert b\rvert \geq 0^{\circ}$ $nWm^{-2}sr^{-1}$	$\lvert b\rvert > 30^{\circ}$ $nWm^{-2}sr^{-1}$	$\lvert b\rvert > 45^{\circ}$ $nWm^{-2}sr^{-1}$
Planck [14]	67.40	6.506	6.959	7.996
Riess [15]	74.03	5.923	6.336	7.280
GM-U_{YF} [18],	70.18	6.248	6.683	7.679
Upper GM-U_{YF}[16], [17]	86.31	5.081	5.434	6.244
Lower Limit [4]	-	7.2		

Upper Limit [4]	-	16

The extinction effect of the galactic disk is crucial for evaluating the flux of the extragalactic background light. At high galactic latitudes ($|b| > 45^{\circ}$), the standard cosmological scenarios and the local GM-U_{YF} model successfully fit the measured values [4]. However, the Upper GM-U_{YF} limit remains below the empirical bounds. Even so, a remnant of the EBL appears to persist due to the contribution of distant sources. These sources are not only distant galaxies, whose flux is redshifted proportionally, but also, and especially, active galactic nuclei (AGN/ Quasars) not considered in the range limited to 50 Mpc.

5 Conclusions

We demonstrate that the quantitative resolution of Olbers' paradox can be constrained by evaluating the intensity of the extragalactic background light, restricted to local conditions (50-MGC), and decoupling the evolutionary functions for galactic demographics ($n(z)$ and $\langle L(z)\rangle$). First, it was verified that the hot Big Bang phenomenology provides the formalism for quantitatively evaluating Olbers' paradox. However, calculations showed that the mere expansion of space and the finite age of the universe are insufficient to reproduce the measured luminosity of the EBL on their own.

Analyzing the local universe ($d < 50$ Mpc) under the premise of a constant numerical density (n_0) and average luminosity ($\langle L_0\rangle$) extrapolated toward the deep universe yields EBL intensity values within observational limits. However, examining the luminosity distribution within this volume reveals significant variance. This dispersion indicates that assuming a uniform mean luminosity is physically inconsistent at cosmological scales, invalidating the simplistic extrapolation of local values and demanding evaluations based on galactic demographic evolution.

Modeling local data through regression functions for $n(z)$ and $\langle L(z)\rangle$ proved insufficient to describe the deep universe. Extrapolating these trends results in a calculated EBL flux an order of magnitude below observations, demonstrating that the behavior of the local neighborhood does not represent the global evolutionary history of galaxies. This discrepancy highlights the necessity of incorporating models from the literature that span higher redshifts to achieve a less biased extrapolation.

Implementing decoupled evolutionary models for star-forming (SF) and quiescent (Q) galaxies adjusted the quantitative EBL values to the same order of magnitude as the observed lower bound. Having reached this level of precision, optical dust extinction in the Milky Way's disk was identified as a defining phenomenological factor. To mitigate this bias, galactic latitude filters ($|b| > 30^{\circ}$ and $|b| > 45^{\circ}$) were applied. Under the principle of large-scale isotropy and homogeneity of the universe, the results were compensated by the corresponding sky coverage factor. The fluxes obtained using the $|b| > 45^{\circ}$ filter converge satisfactorily within the empirical boundaries reported in the observational literature.

It is noteworthy that the theoretical upper limit of the scale-dependent GM-U_{YF} framework ($H_{0,upper} = 86.31$ km s^{-1} Mpc^{-1}) yields a flux marginally below the empirical bounds even under the filter. This implies that modeling the entire universe using a Hubble parameter exclusively valid for asymptotic deep-space expansion—or conversely, purely local kinematics—is an oversimplification. In a strictly scale-dependent cosmology, the true integrated EBL (for GM-U_{YF} framework) must logically lie between the bounding values derived from these two asymptotic extremes.

Data derived from galactic catalogs allow us to infer that the numerical density of galaxies and their mean luminosity produce an integrated radiative flux significantly lower than the average stellar surface brightness. Consequently, the sky remains dark in regions devoid of local sources, even after accounting for galactic extinction effects. Therefore, the integrated EBL flux is convergent and its intensity is less than that of direct stellar sources, quantitatively resolving the divergent integral of Olbers' Paradox.

Despite the agreement with established limits, an unaccounted flux remnant persists, which could be attributed to the contribution of active galactic nuclei (quasars) not represented in the local 50-MGC

sample. We recommend extending this methodology to red and near-infrared bands, given that bolometric contributions from the deep universe are significantly redshifted toward these wavelengths. Finally, we suggest replicating this analysis using deeper galactic surveys, such as the UltraVISTA catalog, to refine the evolutionary modeling of galactic populations.

Acknowledgements

Funding is gratefully acknowledged from the Ministry of Popular Power for Science and Technology through project CFP 20250000038: Large-scale modification of gravity: an alternative to dark matter and dark energy in the universe

References

[1] H. Olbers, "Über die durchsichtigkeit des weltraums," *Astron. Jahrb. 1826*, vol. 51, pp. 110–121, 1826.
[2] Kelvin, Lord, "On ether and gravitational matter through infinite space," *Phil. Mag.*, vol. 2, pp. 161–177, 1901.
[3] T. R. Lauer *et al.*, "New horizons observations of the cosmic optical background," *ApJ*, vol. 906, no. 2, p. 77, 2021.
[4] K. Mattila *et al.*, "Extragalactic background light: A measurement at 400 nm using dark cloud shadow," *MNRAS*, vol. 470, no. 2, pp. 2152–2169, 2017.
[5] R. A. Windhorst *et al.*, "SKYSURF: Constraints on zodiacal light and extragalactic background light," *ApJ*, vol. 164, no. 4, p. 141, 2022.
[6] D. Ohlson *et al.*, "The 50 mpc galaxy catalog (50 MGC)," *ApJ*, vol. 167, no. 1, p. 31, 2024.
[7] Y. J. Peng *et al.*, "Mass and environment as drivers of galaxy evolution in SDSS and zCOSMOS," *ApJ*, vol. 721, no. 1, pp. 193–221, 2010.
[8] O. Ilbert *et al.*, "Mass assembly in quiescent and star-forming galaxies since $z \simeq 4$," *A&A*, vol. 556, p. A55, 2013.
[9] P. Madau and M. Dickinson, "Cosmic star-formation history," *Ann. Rev. Ast. Asp*, vol. 52, pp. 415–486, 2014.
[10] B. M. Tinsley, "Evolution of the stars and gas in galaxies," *Fund. Cosmic Phys.*, vol. 5, pp. 287–388, 1980.
[11] G. Bruzual and S. Charlot, "Stellar population synthesis at the resolution of 2003," *MNRAS*, vol. 344, no. 4, pp. 1000–1028, 2003.
[12] H. Mo, F. C. van den Bosch, and S. D. M. White, *Galaxy formation and evolution*. Cambridge Univ. Press, 2010.
[13] D. M. Scolnic *et al.*, "The complete light-curve sample of spectroscopically confirmed type ia supernovae from pan-STARRS1 and cosmological constraints from the combined pantheon sample," *ApJ*, vol. 859, no. 2, p. 101, 2018.
[14] Planck Collaboration, "Planck 2018 results. VI," *A&A*, vol. 641, p. A6, 2020.
[15] A. G. Riess *et al.*, "Large magellanic cloud cepheid standards provide a 1% foundation for H_0," *ApJ*, vol. 876, no. 1, p. 85, 2019.
[16] N. Falcon, "A large-scale heuristic modification of newtonian gravity," *J. Astrophys. Astr.*, vol. 42, p. 102, 2021.
[17] N. Falcon, "Modified gravitation and mach's principle," *OAJA*, vol. 1, no. 1, p. 000103, 2023.
[18] N. Falcon and A. Aguirre, "Theoretical deduction of the hubble law," *IJAA*, vol. 4, pp. 551–559, 2014.